

Dispersion and lineshape of plasmon satellites in one, two and three dimensions

Derek Vigil-Fowler,¹ Steven G. Louie,² and Johannes Lischner^{3,*}

¹*National Renewable Energy Laboratory, Golden, Colorado 80401, USA.*

²*Department of Physics, University of California at Berkeley and Materials Science Division, Lawrence Berkeley National Laboratory, Berkeley, CA 94720, USA.*

³*Department of Physics and Department of Materials, and the Thomas Young Centre for Theory and Simulation of Materials, Imperial College London, London SW7 2AZ, United Kingdom*

Using state-of-the-art many-body Green's function calculations based on the "GW plus cumulant" approach, we analyze the properties of plasmon satellites in the electron spectral function resulting from electron-plasmon interactions in one-, two- and three-dimensional systems. Specifically, we show how their dispersion relation, lineshape and linewidth are related to the properties of the constituent electrons and plasmons. To gain insight into the many-body processes giving rise to the formation of plasmon satellites, we connect the "GW plus cumulant" approach to a many-body wavefunction picture of electron-plasmon interactions and introduce the coupling-strength weighted electron-plasmon joint-density states as a powerful concept for understanding plasmon satellites.

PACS numbers: 73.22.Pr, 71.15.Qe, 71.45.Gm, 71.10.-w

Introduction.—The interaction of electrons with bosons is of fundamental importance for many phenomena in condensed matter physics, plasma physics and cold atom physics. Recently, there has been great interest in the coupling of electrons and plasmons, which are collective excitations describing quantized oscillations of the charge density. For example, the decay of plasmons into energetic or "hot" electron-hole pairs in metallic surfaces and nanoparticles, which is triggered by electron-plasmon coupling, has led to a new generation of plasmonic devices for photovoltaics and photocatalysis [1–3].

Satellite features in the spectral function of electrons are another consequence of electron-plasmon interactions. Such plasmon satellites have long been known in core-electron photoemission spectra [4, 5]. In recent years, valence band plasmon satellites, which were observed experimentally in three-dimensional metals and semiconductors [6–9], but also in two-dimensional systems, such as doped graphene and semiconductor quantum-well electron gases [10–12], received much attention.

To analyze and design the properties of plasmon satellites for photonics and plasmonics applications, an accurate, material-specific theoretical description of electron-plasmon interactions is needed. This is achieved by the GW plus cumulant (GW+C) approach [13, 14], where the cumulant expansion of the electron Green's function G is truncated at second order in the screened Coulomb interaction W . GW+C calculations yielded good agreement with experimental photoemission and tunneling spectra in a wide range of physical systems [6–8, 15–17] and also with highly accurate coupled-cluster Green's function calculations [18].

While Green's function methods, such as the GW+C approach, often produce highly accurate results, gaining intuition and insights into the underlying many-

body processes can be difficult. In this paper, we develop a complementary many-body wavefunction-based approach for plasmonic (and more generally, bosonic) satellites in the electron spectral function which offers a clear and simple physical picture of electron-plasmon interactions and leads to new insights into the results of GW+C calculations. Specifically, this approach reveals that the concepts of satellite dispersion, satellite lineshape and satellite linewidth are closely related, explains why in three-dimensional materials the plasmon satellite band structure looks like a shifted copy of the quasiparticle band structure and demonstrates that previous models of plasmon satellites in three dimensions are oversimplified and cannot be applied to lower-dimensional systems. We present results for three-dimensional [silicon and the three-dimensional electron gas (3DEG)], two-dimensional (doped graphene) and one-dimensional [the one-dimensional electron gas (1DEG)] systems.

Green's function theory.—The electron spectral function is related to many observables, such as the tunneling and photoemission spectrum, and the contribution $A_{\mathbf{k}}^{\text{IP}}(\omega)$ (with \mathbf{k} denoting the wave vector and we omit a band index) describing the removal of an electron is given by [19, 20]

$$A_{\mathbf{k}}^{\text{IP}}(\omega) = \sum_{\lambda} |\langle N-1, \lambda | c_{\mathbf{k}} | \text{GS} \rangle|^2 \delta(\omega + E_{N-1, \lambda} - E_{\text{GS}}), \quad (1)$$

where $|\text{GS}\rangle$ and E_{GS} denote the ground state wave function and energy of the N -electron system, respectively, and $|N-1, \lambda\rangle$ and $E_{N-1, \lambda}$ denote the eigenstates and energies of the $(N-1)$ -electron system.

The spectral function is related to the one-electron Green's function $G_{\mathbf{k}}(\omega)$ via $A_{\mathbf{k}}(\omega) = 1/\pi \times |\text{Im}G_{\mathbf{k}}(\omega)|$. Within the generalized GW+C approach, the retarded Green's function is expressed as function of time t via

[21]

$$G_{\mathbf{k}}(t) = -i\Theta(t)e^{-iE_{\mathbf{k}}^{\text{HF}}t + C_{\mathbf{k}}(t)}, \quad (2)$$

where $E_{\mathbf{k}}^{\text{HF}}$ denotes the Hartree-Fock orbital energy (given by $E_{\mathbf{k}}^{\text{HF}} = \epsilon_{\mathbf{k}} + \Sigma_{\mathbf{k}}^{\text{X}} - V_{\mathbf{k}}^{xc}$ with $\epsilon_{\mathbf{k}}$, $V_{\mathbf{k}}^{xc}$ and $\Sigma_{\mathbf{k}}^{\text{X}}$ denoting the mean-field orbital energy, the mean-field exchange-correlation potential and the bare exchange self energy, respectively). Also, $C_{\mathbf{k}}(t)$ is the cumulant function given by

$$C_{\mathbf{k}}(t) = \frac{1}{\pi} \int d\omega |\text{Im}\Sigma_{\mathbf{k}}(\omega + E_{\mathbf{k}})| \frac{e^{-i\omega t} + i\omega t - 1}{\omega^2}, \quad (3)$$

where $\Sigma_{\mathbf{k}}(\omega)$ denotes the GW self energy [22, 23] and $E_{\mathbf{k}}$ is the GW quasiparticle energy.

To gain physical understanding, it is useful separate the cumulant function into a satellite contribution $C_{\mathbf{k}}^{\text{sat}}(t)$, which contains the $e^{-i\omega t}$ term in Eq. (3), and a quasiparticle contribution, which contains the $(i\omega t - 1)$ term. Expanding the Green's function in powers of $C_{\mathbf{k}}^{\text{sat}}$ leads to a representation of the spectral function as the sum of a quasiparticle contribution $A_{\mathbf{k}}^{\text{qp}}$ and an infinite series of plasmon satellite contributions $A_{\mathbf{k}}^{(m)}$ (with m denoting the number of plasmons that are created in the shake-up process). Specifically, the first satellite contribution can be expressed as

$$A_{\mathbf{k}}^{(1)}(\omega) = \int d\omega' C_{\mathbf{k}}^{\text{sat}}(\omega - \omega') A_{\mathbf{k}}^{\text{qp}}(\omega'). \quad (4)$$

Approximating $A_{\mathbf{k}}^{\text{qp}}(\omega) \approx Z_{\mathbf{k}}\delta^{(\Gamma)}(\omega - E_{\mathbf{k}})$ with $Z_{\mathbf{k}}$ denoting the renormalization factor and $\delta^{(\Gamma)}$ being a Lorentzian of width Γ , we find that $A_{\mathbf{k}}^{(1)}(\omega) \approx Z_{\mathbf{k}}/\pi \times \text{Im}\Sigma_{\mathbf{k}}(\omega)/(\omega - E_{\mathbf{k}})^2$.

Evaluating Eq. (4) requires the calculation of the imaginary part of the GW self energy. To clarify the physical picture, we use the self energy of a homogeneous electron system in D dimensions with a plasmon-pole model for the dielectric response. With these assumptions, the electron-removal part of the self energy is given by [23]

$$\text{Im}\Sigma_{\mathbf{k}}^{\text{IP}}(\omega) = \frac{\pi}{L^D} \sum_{\mathbf{q}} \lambda_{\mathbf{q}} v_{\mathbf{q}} \delta(\omega - E_{\mathbf{k}-\mathbf{q}} + \omega_{\mathbf{q}}), \quad (5)$$

where $v_{\mathbf{q}}$ denotes the Coulomb interaction in D dimensions and $\omega_{\mathbf{q}}$ and $\lambda_{\mathbf{q}}$ are the plasmon dispersion relation and the plasmon strength, respectively. Also, L is the linear extension of the system and $\mathbf{k} - \mathbf{q}$ corresponds to a hole state.

Inserting Eq. (5) into the expression for $A_{\mathbf{k}}^{(1)}$ yields

$$A_{\mathbf{k}}^{(1)}(\omega) = \frac{Z_{\mathbf{k}}}{L^D} \sum_{\mathbf{q}} \frac{g_{\mathbf{q}}^2}{(E_{\mathbf{k}} - E_{\mathbf{k}-\mathbf{q}} - \omega_{\mathbf{q}})^2} \delta(\omega - E_{\mathbf{k}-\mathbf{q}} + \omega_{\mathbf{q}}), \quad (6)$$

where we introduced the electron-plasmon coupling strength $g_{\mathbf{q}}^2 = \lambda_{\mathbf{q}} v_{\mathbf{q}}$. Eq. (6) shows that the satellite

contribution to the spectral function closely related to the coupling-strength weighted electron-plasmon joint-density of states $J_{\mathbf{k}}(\omega) = 1/L^D \times \sum_{\mathbf{q}} g_{\mathbf{q}}^2 \delta(\omega - E_{\mathbf{k}-\mathbf{q}} + \omega_{\mathbf{q}})$ comprising only plasmon-hole pairs with total momentum \mathbf{k} .

Wavefunction theory.—We will now demonstrate that the expression for the satellite contribution to the spectral function from GW+C [Eq. (6)] can also be derived by considering the effective electron-plasmon Hamiltonian

$$H_{el-pl} = \sum_{\mathbf{k}} E_{\mathbf{k}} c_{\mathbf{k}}^{\dagger} c_{\mathbf{k}} + \sum_{\mathbf{q}} \omega_{\mathbf{q}} a_{\mathbf{q}}^{\dagger} a_{\mathbf{q}} \quad (7)$$

$$+ \sum_{\mathbf{q}, \mathbf{k}} \frac{g_{\mathbf{q}}}{\sqrt{L^D}} c_{\mathbf{k}-\mathbf{q}}^{\dagger} c_{\mathbf{k}} (a_{\mathbf{q}} + a_{-\mathbf{q}}^{\dagger}), \quad (8)$$

where $c_{\mathbf{k}}$ and $a_{\mathbf{q}}$ are destruction operators for quasiparticles and plasmons, respectively. In this Hamiltonian, the first term describes a set of non-interacting quasiparticles, the second term describes a set of non-interacting plasmons (or more generally, bosons) and the third term captures the interaction between quasiparticles and plasmons.

This electron-boson Hamiltonian plays a fundamental role in the theory of electron-phonon interactions, but computing accurate spectral functions is difficult [19, 24, 25]. At intermediate coupling strengths, different types of perturbation theory give significantly different results: When compared to highly accurate path-integral calculations, the self-consistent Brillouin-Wigner perturbation theory yields substantially *worse* results than standard Rayleigh-Schrödinger perturbation theory [19].

For electron-plasmon interactions, Lundqvist demonstrated [24] that the application of Brillouin-Wigner perturbation theory to H_{el-pl} results in the Dyson equation of the GW approach. Solving this equation, he found *two* solutions. While the first solution corresponds to a standard quasiparticle excitation, he assigned the second solution to a novel particle, the *plasmaron*, a strongly coupled, coherent hole-plasmon state. Despite several reports claiming the observation of the plasmaron [10, 11], it has become clear recently that no such excitation exists in known materials and that its spurious prediction signals the inability of the GW method (and, equivalently, the Brillouin-Wigner perturbation theory) to describe plasmon satellites [6, 7, 15, 16].

Motivated by its accurate description of electron-phonon interactions, we now apply Rayleigh-Schrödinger perturbation theory to H_{el-pl} . Without electron-plasmon interactions, i.e. for $g_{\mathbf{q}} = 0$, the eigenstates of the $(N-1)$ -electron system are simply $c_{\mathbf{k}}|\text{GS}\rangle$ (with energy $E_{\text{GS}} - E_{\mathbf{k}}$) and $a_{\mathbf{q}}^{\dagger} c_{\mathbf{k}-\mathbf{q}}|\text{GS}\rangle$ (with energy $E_{\text{GS}} - E_{\mathbf{k}-\mathbf{q}} + \omega_{\mathbf{q}}$) [26]. Only the state $c_{\mathbf{k}}|\text{GS}\rangle$ gives a contribution to Eq. (1) and the resulting spectral function has a single delta-function peak and no satellite features.

Next, we include electron-plasmon interactions us-

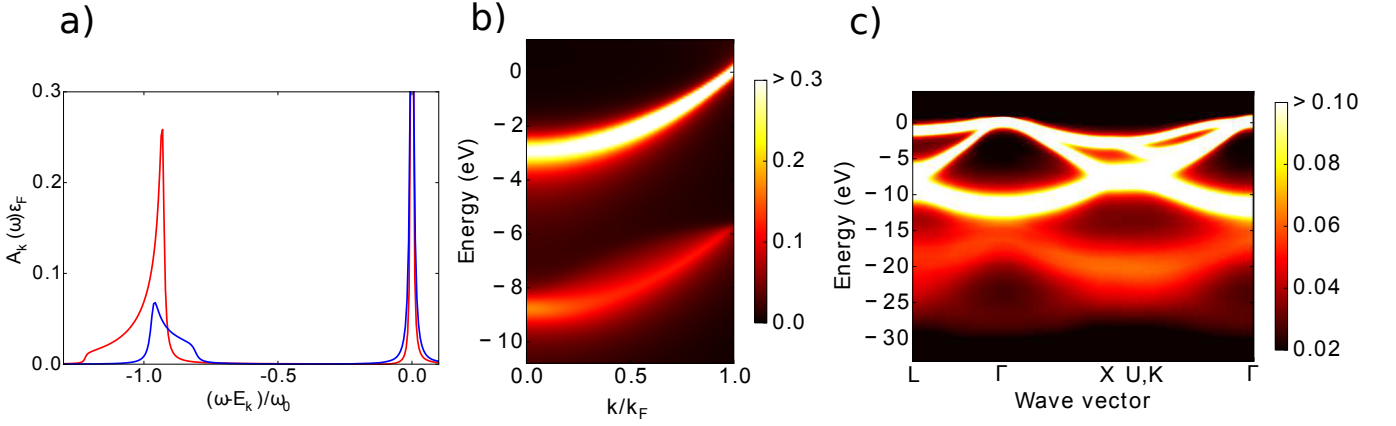


FIG. 1. a) GW plus cumulant spectral functions of the three-dimensional electron gas at $\mathbf{k} = 0$ for $r_s = 1.0$ (red curve) and $r_s = 3.0$ (blue curve). b) Spectral functions (in $1/\text{eV}$) of the three-dimensional electron gas at $r_s = 4.0$ (corresponding to metallic sodium) from GW plus cumulant theory. c) Spectral functions (in $1/\text{eV}$) of silicon from *ab initio* GW plus cumulant theory calculations.

ing first-order Rayleigh-Schrödinger perturbation theory. The non-interacting states that lie in the energy region of the first satellite are the hole-plasmon pairs $a_{\mathbf{q}}^\dagger c_{\mathbf{k}-\mathbf{q}}|\text{GS}\rangle$. Including the hole-plasmon coupling yields

$$a_{\mathbf{q}}^\dagger c_{\mathbf{k}-\mathbf{q}}|\text{GS}\rangle \rightarrow \left[a_{\mathbf{q}}^\dagger c_{\mathbf{k}-\mathbf{q}} + \frac{1}{\sqrt{L^D}} \frac{g_{\mathbf{q}}}{E_{\mathbf{k}} - E_{\mathbf{k}-\mathbf{q}} + \omega_{\mathbf{q}}} c_{\mathbf{k}} + \dots \right] |\text{GS}\rangle, \quad (9)$$

i.e. the hole-plasmon pair state acquires a quasiparticle component, which makes this state “visible” in the spectral function as a satellite structure. Inserting Eq. (9) into Eq. (1), we recover Eq. (6) for the plasmon satellite contribution to the electron spectral function. This analysis shows clearly that no single, coherent hole-plasmon state is formed, but instead the satellite is comprised of a large number of incoherent, weakly interacting hole-plasmon pairs.

Plasmon satellites in three dimensions.—We first study the properties of plasmon satellites in the 3DEG. In this system, the plasmon dispersion is parabolic at small wave vectors, i.e. $\omega_{\mathbf{q}} = \omega_0 + \beta q^2$ [20] and we assume that also the quasiparticle dispersion is parabolic, i.e. $E_{\mathbf{k}} = \alpha k^2$.

With these assumptions, we can *analytically* compute the coupling-constant weighted electron-plasmon joint density of states, which is closely related to the satellite contribution $A_{\mathbf{k}}^{(1)}(\omega)$ to the spectral function [27]. For $\mathbf{k} = 0$, we find

$$J_{\mathbf{k}=0}(\omega) = \frac{\omega_0}{2\pi} \frac{\Theta(\text{sgn}(\alpha - \beta)[\omega + \omega_0])}{\sqrt{|(\alpha - \beta)(\omega + \omega_0)|}}. \quad (10)$$

This result shows that the satellite feature is peaked at $\omega = -\omega_0$, i.e. the satellite is shifted from the quasiparticle energy by the lowest plasmon energy ω_0 . Moreover, the satellite exhibits a highly *asymmetric* lineshape,

which depends sensitively on the *relative magnitudes of the plasmon and quasiparticle effective masses* [given by $m_{pl}^* = 1/(2\beta)$ and $m_{qp}^* = 1/(2\alpha)$, respectively]: if β is larger α , the satellite peak has a tail towards higher binding energies (i.e. away from the Fermi energy). If α is greater than β , the tail is towards lower binding energies. If the effective masses are equal, the satellite structure is symmetric.

Equation (10) predicts the occurrence of a drastic change in the satellite lineshape as function of the Wigner-Seitz radius r_s . While the quasiparticle effective mass only has a weak dependence on r_s and may be approximated by its non-interacting value, i.e. $\alpha = 0.5$ (in atomic units) [23], the plasmon effective mass depends sensitively on r_s . Within the random-phase approximation (RPA), we find $\beta \approx 0.64/\sqrt{r_s}$ [20]. At small r_s , β is large and the tail of the satellite extends to higher binding energies. For $r_s \gtrsim 1.6$, β is smaller than α and the tail of the satellite extends to lower binding energies. Figure 1(a) shows the GW+C spectral functions for the 3DEG with $r_s = 1.0$ and $r_s = 3.0$ obtained with a plasmon-pole model. It can clearly be seen that the tails of the satellites extend into different directions.

In combination with angle-resolved photoemission spectroscopy (ARPES), the above analysis imposes useful limits on the value of the plasmon effective mass. While ARPES experiments do not measure the plasmon dispersion, they can determine both the quasiparticle effective mass and the satellite lineshape. Depending on the direction of the satellite tail [see Fig. 1(a)], the plasmon effective mass must be either smaller or larger than the quasiparticle effective mass. This approach is particularly useful in multiband systems, where each band leads to an additional constraint on the plasmon effective mass.

The satellite lineshape from *full* GW+C calculations

is more symmetric than predicted by Eq. (10) since additional broadening mechanisms arising from finite quasiparticle linewidths [see Eq. (4)] and finite plasmon linewidths (for example, caused by Landau damping [28]) are taken into account. The total linewidth of the satellite may thus be approximated as the sum of the widths of the coupling-strength weighted hole-plasmon joint density of states, the quasiparticle spectral function and the plasmon lineshape. In spectroscopic experiments on real samples, additional phonon and disorder broadening as well as broadening due to extrinsic losses occur [29, 30].

Also at nonzero wave vectors, the peak of $J_{\mathbf{k}}(\omega)$ is located at an energy ω_0 below the quasiparticle energy $E_{\mathbf{k}}$ (see appendix). In other words: the satellite band is a rigidly shifted copy of the quasiparticle band. Surprisingly, this means that the *effective mass of the satellite is the same as the quasiparticle effective mass* irrespective of the plasmon effective mass. We confirm our conclusions by carrying out GW+C calculations of the 3DEG at $r_s = 4.0$ (corresponding to metallic sodium) using the frequency-dependent RPA dielectric function, see Fig. 1(b).

Generalizing our findings for the plasmon satellite properties of the 3DEG to real materials is straightforward. Fig. 1(c) shows the spectral functions of crystalline silicon obtained from *ab initio* GW+C calculations [31]. Because of the parabolic dispersion of the valence quasiparticle bands near the band extrema and the parabolic dispersion of the plasmon, the plasmon satellite band structure appears as a rigidly shifted copy of the quasiparticle band structure, but significantly broadened.

Previous models of plasmon satellites in three-dimensional systems [6, 32, 33] assumed that plasmon dispersion is a minor effect and approximated the satellite simply as a shifted, broadened copy of the quasiparticle peak. Such approaches fail to describe the asymmetric lineshape of the satellite and also cannot be applied straightforwardly to lower-dimensional systems, which we discuss below.

Plasmon satellites in two and one dimensions.—In three-dimensional systems, the satellite feature is separated from the quasiparticle peak by the lowest plasmon frequency. In metallic *two-dimensional* systems, the plasmon energy is proportional to the square root of the plasmon wave vector, i.e. $\omega_q = \beta\sqrt{q}$ [20], and it is not a priori clear where the satellite peak is located.

We now apply our GW+C-based analysis of plasmon satellite properties to *two-dimensional systems* and choose electron-doped graphene as a test case. Within the Dirac model approach, the two bands in the vicinity of the Fermi energy are described by a linear dispersion relation, i.e. $E_{\mathbf{k}} = \pm v_F k$ with v_F denoting the graphene Fermi velocity. Here, \mathbf{k} is measured from the K or K' points of the graphene Brillouin zone.

Taking into account that electrons in the upper Dirac band give the dominant contribution to the satellite

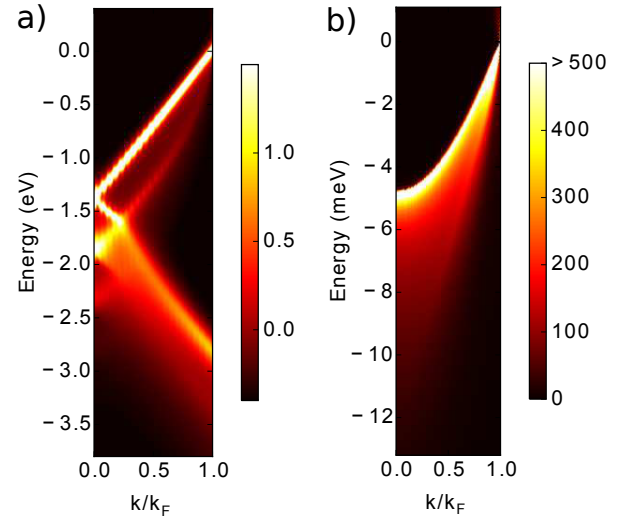


FIG. 2. a) Spectral functions (in 1/eV) of doped graphene on a silicon carbide substrate from GW plus cumulant theory. b) Spectral functions (in 1/eV) of a one-dimensional electron gas from GW plus cumulant theory.

spectral function at the Dirac point [34], we find that $J_{\mathbf{k}=0}(\omega) \propto \Theta(\omega + \tilde{\omega})/\sqrt{\omega + \tilde{\omega}}$, where $\tilde{\omega} = \beta^2/(4v_F)$ is the separation between the quasiparticle and satellite peaks. Again, the plasmon satellite lineshape is highly asymmetric. The dependence of β on the charge density n , $\beta \propto \sqrt{n}$ [16], gives rise to small changes in the lineshape as function of the carrier density. Comparing the expression for $J_{\mathbf{k}=0}$ of doped graphene to the result for the 3DEG [see Eq. (10)], we observe that no drastic changes in the asymmetry of the lineshape occur as function of the carrier density.

Figure 2(a) shows the spectral functions of doped graphene on a silicon carbide substrate from GW+C calculations [35]. We observe that the plasmon satellite band is not a shifted copy of the quasiparticle band, but that the two bands merge at the Fermi wave vector k_F .

Finally, we analyze the plasmon satellite properties in a *one-dimensional* metallic system, the 1DEG. In this system, the plasmon dispersion relation at long wavelengths is given by $\omega_q = \beta q \sqrt{\log(1/ql)}$ with l denoting a cutoff distance [36–38]. Assuming a parabolic quasiparticle dispersion, i.e. $E_{\mathbf{k}} = \alpha k^2$, we find again that the first plasmon satellite exhibits a highly asymmetric lineshape. Fig. 2(b) shows GW+C spectral functions for the 1DEG at $r_s = 1.4$ [39]. In contrast to graphene and the 3DEG, the plasmon satellite is relatively weak and appears as a shoulder-like feature near a strong quasiparticle band.

Summary.—By connecting the GW+C Green’s function approach to a wavefunction-based perspective, we established the coupling-constant weighted electron-plasmon joint density of states $J_{\mathbf{k}}(\omega)$ as a useful quantity for analyzing plasmon satellites in electron spectral functions. We evaluated $J_{\mathbf{k}}(\omega)$ for systems in one, two

and three dimensions and demonstrated how the properties of plasmon satellites are related to the properties of the underlying electrons and plasmons emphasizing the importance of plasmon dispersion. Our formalism for electron-plasmon interactions can be generalized straightforwardly to study the generation of hot electron-hole pairs in plasmonic devices for photovoltaics and photocatalysis in the future.

Acknowledgments.—The authors would like to thank Prof. Feliciano Giustino for valuable discussions. J.L. acknowledges support from EPSRC under Grant No. EP/N005244/1 and also from the Thomas Young Centre under Grant No. TYC-101. Via J.L.'s membership of the UK's HEC Materials Chemistry Consortium, which is funded by EPSRC (EP/L000202), this work used the ARCHER UK National Supercomputing Service. S.G.L. acknowledges support from the National Science Foundation under grant DMR15-1508412.

APPENDIX

Electron-Plasmon Joint Density of States in Three Dimensions.—We calculate the coupling-strength weighted joint density of states $J_{\mathbf{k}}(\omega)$ comprising only plasmon-hole pairs with total momentum \mathbf{k} for a three-dimensional homogeneous electron gas (3DEG). As shown in the main text, this quantity is closely related to the first satellite contribution to the electron spectral function. Specifically, $J_{\mathbf{k}}(\omega)$ is given by

$$J_{\mathbf{k}}(\omega) = \int \frac{d^3q}{(2\pi)^3} g_{\mathbf{q}}^2 \delta(\omega - E_{\mathbf{k}-\mathbf{q}} + \omega_{\mathbf{q}}), \quad (11)$$

where $g_{\mathbf{q}}$ denotes the electron-plasmon coupling strength, $\omega_{\mathbf{q}} = \omega_0 + \beta q^2$ is the plasmon dispersion and $E_{\mathbf{k}} = \alpha k^2$ is the quasiparticle dispersion.

Using a plasmon-pole model that conserves sum rules, we find $g_{\mathbf{q}}^2 = v_{\mathbf{q}} \omega_0^2 / (2\omega_{\mathbf{q}}) \approx v_{\mathbf{q}} \omega_0 / 2$ with $v_{\mathbf{q}} = 4\pi/q^2$.

For the special case of $\mathbf{k} = 0$, we find

$$\begin{aligned} J_{\mathbf{k}=0}(\omega) &= \frac{\omega_0}{\pi} \int_0^\infty dq \delta(\omega + \omega_0 - [\alpha - \beta]q^2) \\ &= \frac{\omega_0}{2\pi} \frac{\Theta(\text{sgn}(\alpha - \beta)(\omega + \omega_0))}{\sqrt{|(\alpha - \beta)(\omega + \omega_0)|}}, \end{aligned} \quad (12)$$

which has a peak at $-\omega_0$.

In the general case of nonzero \mathbf{k} , we have to evaluate

$$\begin{aligned} J_{\mathbf{k}}(\omega) &= \\ \frac{\omega_0}{2\pi} \int_0^\infty dq \int_{-1}^1 du \delta(\omega + \omega_0 - \alpha k^2 + 2\alpha k u + [\beta - \alpha]q^2). \end{aligned} \quad (13)$$

Using that $\int_{-1}^1 du \delta(A + Bu) = \Theta(|B| - |A|)/|B|$, we

find that

$$\begin{aligned} J_{\mathbf{k}}(\omega) &= \\ \frac{\omega_0}{4\pi|\alpha|k} \int_0^\infty \frac{dq}{q} \Theta(2kq|\alpha| - |\omega + \omega_0 - \alpha k^2 + [\beta - \alpha]q^2|). \end{aligned} \quad (14)$$

We now assume that $\beta - \alpha > 0$ and distinguish the two cases: i) $\omega_k^* \equiv \omega + \omega_0 - \alpha k^2 > 0$ and ii) $\omega_k^* < 0$. To find the position of the peak of $J_{\mathbf{k}}(\omega)$, it is sufficient to consider case i) and we find that

$$\begin{aligned} J_{\mathbf{k}}(\omega) &= \frac{\omega_0}{4\pi|\alpha|k} \int_0^\infty \frac{dq}{q} \Theta(2kq|\alpha| - \omega_k^* - [\beta - \alpha]q^2) \\ &= \frac{\omega_0}{4\pi|\alpha|k} \Theta(1 - f_k) \log \left[\frac{1 + \sqrt{1 - f_k}}{1 - \sqrt{1 - f_k}} \right], \end{aligned} \quad (15)$$

with $f_k = [\beta - \alpha]\omega_k^*/(k|\alpha|)^2$. This function diverges as $\omega_k^* \rightarrow 0$ indicating that $J_{\mathbf{k}}(\omega)$ is peaked at $-\omega_0 - \alpha k^2$.

For case ii), we have to evaluate

$$\begin{aligned} J_{\mathbf{k}}(\omega) &= \frac{\omega_0}{4\pi|\alpha|k} \left[\int_0^{q^*} \frac{dq}{q} \Theta(2kq|\alpha| + \omega_k^* + [\beta - \alpha]q^2) + \right. \\ &\quad \left. \int_{q^*}^\infty \frac{dq}{q} \Theta(2kq|\alpha| - \omega_k^* - [\beta - \alpha]q^2) \right] \\ &= \frac{\omega_0}{4\pi|\alpha|k} \log \left[\frac{1 + \sqrt{1 - f_k}}{-1 + \sqrt{1 - f_k}} \right], \end{aligned} \quad (16)$$

with $q^* = \sqrt{|\omega_k^*|/[\beta - \alpha]}$.

Note that the solutions above also describe the case of $\beta - \alpha < 0$, but now Eq. (5) describes negative ω_k^* and Eq. (6) describes positive ω_k^* .

* jlischners597@gmail.com

- [1] S. Mukherjee, F. Libisch, N. Large, O. Neumann, L. V. Brown, J. Cheng, J. B. Lassiter, E. A. Carter, P. Nordlander, and N. J. Halas, *Nano Letters* **13**, 240 (2012).
- [2] C. Clavero, *Nature Photonics* **8**, 95 (2014).
- [3] M. Moskovits, *Nature Nanotechnology* **10**, 6 (2015).
- [4] B. Lundqvist, *Physik der kondensierten Materie* **9**, 236 (1969).
- [5] J. Inglesfield, *Journal of Physics C: Solid State Physics* **16**, 403 (1983).
- [6] M. Guzzo, G. Lani, F. Sottile, P. Romaniello, M. Gatti, J. J. Kas, J. J. Rehr, M. G. Silly, F. Sirotti, and L. Reining, *Phys. Rev. Lett.* **107**, 166401 (2011).
- [7] J. Lischner, G. Pálsson, D. Vigil-Fowler, S. Nemsak, J. Avila, M. Asensio, C. Fadley, and S. G. Louie, *Physical Review B* **91**, 205113 (2015).
- [8] M. Guzzo, J. J. Kas, L. Sponza, C. Giorgetti, F. Sottile, D. Pierucci, M. G. Silly, F. Sirotti, J. J. Rehr, and L. Reining, *Physical Review B* **89**, 085425 (2014).
- [9] L. Ley, S. Kowalczyk, R. Pollak, and D. Shirley, *Physical Review Letters* **29**, 1088 (1972).

- [10] A. Bostwick, F. Speck, T. Seyller, K. Horn, M. Polini, R. Asgari, A. H. MacDonald, and E. Rotenberg, *Science* **328**, 999 (2010).
- [11] O. E. Dial, R. C. Ashoori, L. N. Pfeiffer, and K. W. West, *Phys. Rev. B* **85**, 081306(R) (2012).
- [12] A. L. Walter, A. Bostwick, K.-J. Jeon, F. Speck, M. Ostler, T. Seyller, L. Moreschini, Y. J. Chang, M. Polini, R. Asgari, *et al.*, *Physical Review B* **84**, 085410 (2011).
- [13] D. C. Langreth, *Phys. Rev. B* **1**, 471 (1970).
- [14] L. Hedin, *Physica Scripta* **21**, 477 (1980).
- [15] J. Lischner, D. Vigil-Fowler, and S. G. Louie, *Physical Review Letters* **110**, 146801 (2013).
- [16] J. Lischner, D. Vigil-Fowler, and S. G. Louie, *Physical Review B* **89**, 125430 (2014).
- [17] F. Aryasetiawan, L. Hedin, and K. Karlsson, *Phys. Rev. Lett.* **77**, 2268 (1996).
- [18] J. McClain, J. Lischner, T. Watson, D. A. Matthews, E. Ronca, S. G. Louie, T. C. Berkelbach, and G. K. Chan, arXiv preprint arXiv:1512.04556 (2015).
- [19] G. D. Mahan, *Many-Particle Physics* (Springer Science & Business Media, 2013).
- [20] G. Giuliani and G. Vignale, *Quantum Theory of the Electron Liquid* (Cambridge University Press, 2005).
- [21] J. Kas, J. J. Rehr, and L. Reining, *Physical Review B* **90**, 085112 (2014).
- [22] L. Hedin, B. Lundqvist, and S. Lundqvist, *Solid State Communications* **5**, 237 (1967).
- [23] L. Hedin and S. Lundqvist, *Solid State Physics* **23**, 1 (1969).
- [24] B. I. Lundqvist, *Phys. Kondens. Mater.* **6**, 193 (1967).
- [25] L. Hedin, *J. Phys.: Condens. Matter* **11**, 489 (1999).
- [26] We neglect states with more than one plasmon excitation.
- [27] See supplementary materials for details.
- [28] K. Sturm, *Advances in Physics* **31**, 1 (1982).
- [29] C.-O. Almbladh and L. Hedin, *Handbook of Synchrotron Radiation*, Vol. 1 (E. E. Koch (North-Holland, Amsterdam), 1983) p. 686.
- [30] L. Hedin, J. Michiels, and J. Inglesfield, *Physical Review B* **58**, 15565 (1998).
- [31] Our calculations employ a DFT-LDA mean-field starting point (obtained using the QUANTUM ESPRESSO program package[40]) and a full-frequency treatment of the dielectric matrix. Self-energy calculations were carried out using the BerkeleyGW program package [41]. We employ a $8 \times 8 \times 8$ k-point grid, a 5 Ry dielectric cutoff and sampled frequencies up to 300 eV.
- [32] F. Caruso and F. Giustino, *Physical Review B* **92**, 045123 (2015).
- [33] F. Caruso, H. Lambert, and F. Giustino, *Physical Review Letters* **114**, 146404 (2015).
- [34] M. Polini, R. Asgari, G. Borghi, Y. Barlas, T. Pereg-Barnea, and A. MacDonald, *Physical Review B* **77**, 081411 (2008).
- [35] Our calculations employ a Dirac-model starting point and use the frequency-dependent RPA dielectric constant of doped graphene [42]. For the dielectric response of the silicon carbide substrate, we use the approach of Ref. [15]. The Fermi energy is $\epsilon_F = 1$ eV.
- [36] A. Sommerfeld, *Annalen der Physik und Chemie* **67**, 233 (1899).
- [37] B. Y.-K. Hu and S. D. Sarma, *Physical Review B* **48**, 5469 (1993).
- [38] A. Chaplik and M. Krasheninnikov, *Surface Science* **98**, 533 (1980).
- [39] We employ a one-dimensional Coulomb interaction corresponding to a cylindrical system of radius 100 Å, an effective mass of $m^* = 0.067$ (in atomic units) and a background dielectric constant of 12.7 corresponding to a gallium arsenide quantum-wire structure [37].
- [40] P. Giannozzi, S. Baroni, N. Bonini, M. Calandra, R. Car, C. Cavazzoni, D. Ceresoli, G. L. Chiarotti, M. Cococcioni, I. Dabo, A. Dal Corso, S. de Gironcoli, S. Fabris, G. Fratesi, R. Gebauer, U. Gerstmann, C. Gougoussis, A. Kokalj, M. Lazzeri, L. Martin-Samos, N. Marzari, F. Mauri, R. Mazzarello, S. Paolini, A. Pasquarello, L. Paulatto, C. Sbraccia, S. Scandolo, G. Sclauzero, A. P. Seitsonen, A. Smogunov, P. Umari, and R. M. Wentzcovitch, *J. Phys.: Condens. Matter* **21**, 395502 (2009).
- [41] J. Deslippe, G. Samsonidze, D. A. Strubbe, M. Jain, M. L. Cohen, and S. G. Louie, *Comput. Phys. Commun.* **183**, 1269 (2012).
- [42] B. Wunsch, T. Stauber, F. Sols, and F. Guinea, *New J. Phys.* **8**, 318 (2006).